Effect of Molecular Structure of α,α′-Dialkylquaterthiophenes and Their Organosilicon Multipods on Ordering, Phase Behavior, and Charge Carrier Mobility

ARTICLE *in* THE JOURNAL OF PHYSICAL CHEMISTRY C · OCTOBER 2012

Impact Factor: 4.77 · DOI: 10.1021/jp307054r

14 AUTHORS, INCLUDING:

Mourran Ahmed
RWTH Aachen University
62 PUBLICATIONS **998** CITATIONS
SEE PROFILE

Yuriy N. Luponosov
Institute of Synthetic Polymeric Materials
38 PUBLICATIONS **331** CITATIONS
SEE PROFILE

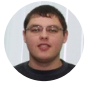

O. V. Borshchev
Institute of Synthetic Polymeric Materials
25 PUBLICATIONS **235** CITATIONS
SEE PROFILE

Sergei Ponomarenko
Institute of Synthetic Polymeric Materials
119 PUBLICATIONS **2,191** CITATIONS
SEE PROFILE

THE JOURNAL OF PHYSICAL CHEMISTRY C

Article

pubs.acs.org/JPCC

Effect of Molecular Structure of α,α′-Dialkylquaterthiophenes and Their Organosilicon Multipods on Ordering, Phase Behavior, and Charge Carrier Mobility

Denis.V. Anokhin,[†,‡] Matthieu Defaux,[§] Ahmed Mourran,[§] Martin Moeller,[§] Yury N. Luponosov,[†,∥] Oleg V. Borshchev,[†,∥] Artem V. Bakirov,[†,∥] Maxim A. Shcherbina,[†,∥] Sergei N. Chvalun,[∥] Timo Meyer-Friedrichsen,[⊥] Andreas Elschner,[⊥] Stephan Kirchmeyer,[⊥] Sergei A. Ponomarenko,*[,†,∥] and Dmitri A. Ivanov*[,†,‡]

[†]Moscow State University, Faculty of Fundamental Physical and Chemical Engineering, GSP-1, 1-51 Leninskie Gory, Moscow, 119991, Russian Federation

[‡]Institut de Sciences des Matériaux de Mulhouse (CNRS LRC 7228), 15 rue Jean Starcky, B.P 2488, Mulhouse, 68057, France

[§]DWI an der RWTH Aachen e.V., Pauwelsstr. 8, Aachen, D-52074, Germany

[∥]Enikolopov Institute of Synthetic Polymeric Materials, Russian Academy of Sciences, 70 ul. Profsoyuznaya, Moscow, 117393, Russian Federation

[⊥]Heraeus Precious Metals GmbH & Co. KG, Conductive Polymers Division (Clevios), Chempark Leverkusen, Bldg. B202, Leverkusen, D-51368, Germany

Supporting Information

ABSTRACT: We report on bulk structures of a family of quaterthiophene (**4T**) derivatives with linear and branched end groups such as α,α′-dihexylquaterthiophene (**Hex-4T-Hex**), α,α′-didecyl-quaterthiophene (**Dec-4T-Dec**) and α,α′-bis(2-ethylhexyl)quaterthiophene (**EH-4T-EH**), tetramethyldisiloxane-based dimers **D2-Und-4T-EH** and **D2-Und-4T-Hex**, and carbosilane-siloxane-based tetramers **D4-Und-4T-EH** and **D4-Und-4T-Hex**. The dimers and tetramers contain undecylenic (**Und**) spacers between the disiloxane and **4T**- units of the molecule. The impact of the molecular architecture on the bulk structure at different temperatures is addressed with X-ray diffraction and differential scanning calorimetry. For all of the studied quaterthiophene-containing organosilicon multipods the formation of **4T**-crystal sublattice is observed. The alkyl periphery plays an important role in the molecular packing and thermal stability of the ordered phase. They can stabilize or destabilize the crystal phase, depending on their length and architecture. The quaterthiophenes with 2-ethylhexyl end groups adopt a zig-zag conformation in the crystalline state at room temperature. This change of conformation leads to a significant decrease of the polymorphic transition and isotropization temperatures. The efficiency of **4T** packing in the sublattice is estimated from the molecular cross-section (S) in the plane normal to the molecular axis. Correlations between S and field-effect charge carrier mobility are established.

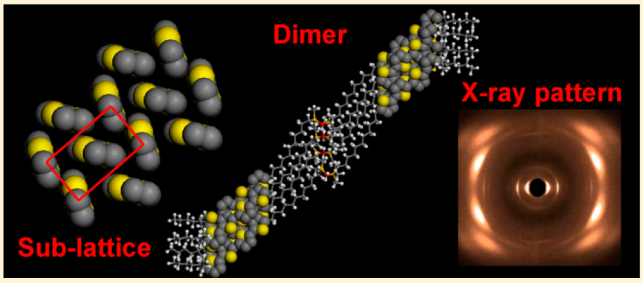

INTRODUCTION

During the last decades, oligo- and polythiophenes have been attracting much attention due to their interesting (semi)-conducting and optical properties,[1] which can be utilized in novel organic electronic devices such as organic field-effect transistors (OFETs), organic photovoltaic cells (OPV cells), organic light emitting diodes (OLEDs), electronic sensors, and others.[2] As contrasted to polythiophenes with polydispersity typical of polymers, oligothiophenes are characterized by a strictly uniform molecular structure, which allows for better and simpler purification and gives rise to improved semiconducting properties.[3] The main semiconducting characteristic of organic electronic materials, i.e., charge carrier mobility, is known to enhance with increasing the conjugation length and crystallinity of oligothiophenes.[4] However, simultaneously with this increase, the solubility of the compounds significantly decreases, which typically leads to vacuum sublimation requirement for their processing. Yet solution processing is the most desirable technique for organic electronics due to its simplicity and relatively low cost.

To improve the solubility and solution processability of oligothiophenes, their molecular structure can be modified with different substituents either in α- or in β-positions of the thiophene ring. It has been shown that β-substituents can

Received: July 16, 2012
Revised: October 8, 2012
Published: October 9, 2012

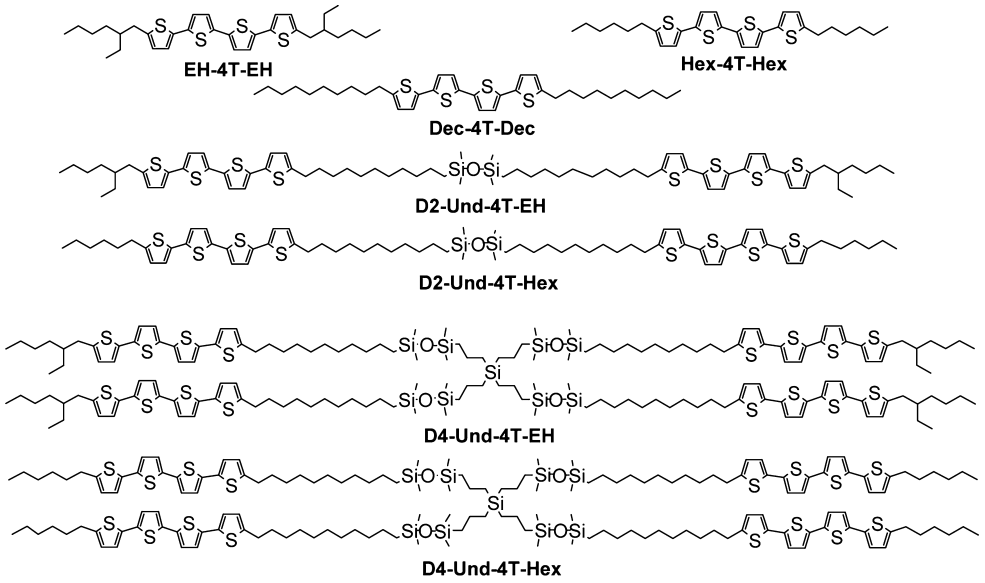

Figure 1. Chemical structures of α,α'-bis(2-ethylhexyl) quaterthiophene (**EH-4T-EH**), α,α'-dihexylquaterthiophene (**Hex-4T-Hex**) and α,α'-didecylquaterthiophene (**Dec-4T-Dec**), 2-ethylhexyl end-capped tetramethyldisiloxane dimer (**D2-Und-4T-EH**) and carbosilane-siloxane tetramer (**D4-Und-4T-EH**), as well as hexyl end-capped tetramethyldisiloxane dimer (**D2-Und-4T-Hex**) and carbosilane-siloxane tetramer (**D4-Und-4T-Hex**) investigated in this work.

significantly improve the solubility, but can at the same time decrease the molecular order and hence the charge carrier mobility.[5] The α-substituents can also increase the solubility, albeit not so strongly, which can still result in high mobility materials.[3] In order to find a reasonable compromise between solubility and crystallinity, different bulky and/or branched groups have been used as α-substituents for oligothiophenes.[6] Nowadays, a large number of oligothiophene-based complex molecular architectures have been designed and investigated.[7] Many of them show good semiconducting, light harvesting, or light emitting properties that make them promising functional materials for OFETs,[8] OPV cells,[9] or OLEDs.[10] Combination of oligothiophenes with organosilicon groups leads to the design of different solution-processable linear, branched or dendritic architectures with interesting optical and electrical properties.[11]

Quaterthiophene (**4T**) and its α,α'-dialkylsubstituted derivatives are the smallest oligothiophenes showing high field-effect mobility in OFETs.[3] Moreover, it was shown that a **4T**-based tetramer with organosilicon core and linear hexyl end groups **D4-Und-4T-Hex** (cf. Figure 1) shows good semiconducting properties in solution-processable OFETs,[12] while their analogues with branched 2-ethylhexyl end-capping groups **D2-Und-4T-EH** and **D4-Und-4T-EH** (cf. Figure 1) are more suitable as donor materials in bulk heterojunction OPV cells.[13] However, **D4-Und-4T-Hex** exhibits only a very low efficiency in OPV cells, while **D2-Und-4T-EH** and **D4-Und-4T-EH** show very low mobility in OFETs. This behavior was tentatively attributed, on the one hand, to a better solubility of 2-ethylhexyl end-capped materials, which is crucial for OPV cells, and, on the other hand, to different ordering of the multipods end-capped with linear hexyl and branched 2-ethylhexyl groups.

Despite pronounced interest in the quaterthiophene derivatives, the information on their structure remains quite limited. In general, it is considered that oligothiophene blocks tend to segregate, forming the characteristic sublattice with "herring-bone" packing.[14] The sublattice contains two molecules, with the parameters being usually close to that for nonsubstituted polythiophene: a = 7.83 Å, b = 5.52 Å. On the WAXS patterns, the formation of regular domains of **4T** is revealed by a set of three characteristic reflections: d_{110} = 4.51 Å, d_{200} = 3.92 Å, and d_{210} = 3.19 Å.

The crystal structure of α,α'-dihexylquaterthiophene **Hex-4T-Hex** was studied previously.[15] At room temperature, **Hex-4T-Hex** forms a monoclinic crystal phase[16] with the following parameters: a = 19.68 Å, b = 11.45 Å, c = 7.35 Å, γ = 92.7°. One unit cell accommodates two molecules in the extended conformation (cf. Figure 2a), in which the **4T**-blocks form

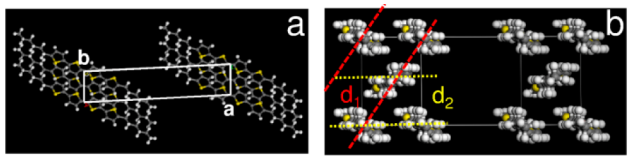

Figure 2. Model of the unit cell of **Hex-4T-Hex**: ab-projection (a) and view parallel to the quaterthiophene block (b). The reticular planes with interplanar spacings d_1 and d_2 are indicated by dashed and dotted lines, respectively.

the above-mentioned "herring-bone" packing (Figure 2b). Differential scanning calorimetry (DSC) data reveal two endothermic transitions at 81 and 180 °C (cf. ref 3a, b and Table 1), which are assigned to a crystal-smectic transition and the isotropization, respectively. For other materials investigated in this paper, no structural investigations have been reported so far.

In the present work, we address the bulk structures of the family of **4T**-derivatives with linear and branched end groups such as α,α'-dihexylquaterthiophene **Hex-4T-Hex**, α,α'-didecylquaterthiophene **Dec-4T-Dec** and α,α'-bis(2-ethylhexyl)-quaterthiophene **EH-4T-EH**, tetramethyldisiloxane-based dimers **D2-Und-4T-EH** and **D2-Und-4T-Hex**, and carbosilane-siloxane-based tetramers **D4-Und-4T-EH** and **D4-Und-4T-Hex** (cf. Figure 1). Both dimers and tetramers contain undecylenic spacers between the disiloxane and **4T** fragments

dx.doi.org/10.1021/jp307054r | J. Phys. Chem. C 2012, 116, 22727−22736

Table 1. Thermodynamic and Structural Parameters of the Studied Quaterthiophene Derivatives

sample	form I	T_{tr} [°C] (ΔH_{tr} [Jg^{-1}])	form II	T_{tr} [°C] (ΔH_{tr} [Jg^{-1}])
Hex-4T-Hex[a]	a = 28.49 Å, b = 6.09 Å, c = 7.81 Å, γ = 91.9°	81 (31.9)	a = 27.15 Å, b = 6.35 Å, c = 8.44 Å, γ = 94.6°	181 (61.6)
Dec-4T-Dec[a]	a = 37.93 Å, b = 5.99 Å; c = 7.79 Å, γ=93.2°	98 (68.5)	a = 36.01 Å, b = 5.91 Å, c = 7.98 Å, γ = 100.9°	168 (60.5)
EH-4T-EH	a = 19.68 Å, b = 11.45 Å, c = 7.35 Å, γ = 92.7°	34(4.9)	a = 19.28 Å, b = 11.62 Å, c = 7.64 Å, γ = 93.1°	108(63.9)
D2-Und-4T-Hex	ordered smectic phase phase a = 73.7 Å	75 (6.2)	disordered smectic phase a = 40.5 Å	190 (54.6)
D2-Und-4T-EH	ordered smectic phase a = 60.44 Å,	98 (21.7)	disordered smectic phase a = 30.84 Å,	136 (42.9)
D4-Und-4T-Hex	ordered smectic phase a = 79.4 Å	160(4.2)	disordered smectic phase a = 46.1 Å,	187(34.6)
D4-Und-4T-EH	ordered smectic phase a = 53.7 Å	102 (15.9)	disordered smectic phase a = 37.8 Å	115 (6.9)

[a]Calorimetric data for **Hex-4T-Hex** and **Dec-4T-Dec** are taken from refs 15 and 17, respectively.

of the molecule. The studied compounds combine a strong tendency of **4T** moieties to crystallize, the segregation between semiconducting **4T** fragments and insulating organosilicon cores, and frustration during the structure formation due to the presence of branched inner core and linear or branched alkyls at the periphery.

The main focus of this work is on elucidating the impact of the molecular architecture (i.e., molecular size and flexibility, number of the quaterthiophene blocks in the molecule, and topology of the peripheral groups) on the structures formed by quaterthiophene-based molecules. Since the optoelectronic properties of the oligothiophene-based active layer in organic electronic devices are crucially dependent on details of the molecular arrangement such as the oligothiophene core packing and tilt angle of the oligothiophene blocks, we specifically address these parameters with X-ray diffraction (XRD). In particular, we search for a relationship between the local molecular ordering of quaterthiophene blocks and the material electronic properties.

EXPERIMENTAL SECTION

Materials. **Hex-4T-Hex** and **Dec-4T-Dec** were synthesized according to the methods described previously.[17] Synthesis of tetramer **D4-Und-4T-Hex** is described in ref 12, synthesis of dimer **D2-Und-4T-EH** and tetramer **D4-Und-4T-EH** is given in ref 13.

Synthesis. 5,5‴-*bis*(2-ethylhexyl)-2,2′:5′,2″:5″,2‴-quaterthiophene (**EH-4T-EH**) was synthesized from 5-(2-ehylhexyl)-5′-bromo-2,2′-bithiophene according to the following scheme:

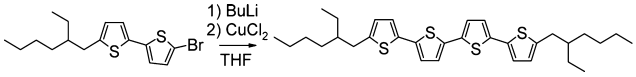

The detailed synthetic procedure is described below:

A 1.6 M solution of butyllithium (2.27 mL, 3.6 mmol) in hexane was added dropwise to a solution of 5-bromo-5′-(2-ethylhexyl)-2,2′-bithiophene (1.30 g, 3.6 mmol) in 40 mL of THF, while the temperature was kept between −70 and −75 °C. The reaction mixture was stirred for 60 min at −75 °C. Then anhydrous copper(II) chloride (0.49 g, 1.8 mmol) was added. The reaction mixture was stirred for 1 h at −78 °C, the cooling bath was removed, and the stirring was continued for 2 h. After completion of the reaction, 200 mL of freshly distilled diethyl ether and 100 mL of water were added. The organic phase was separated, washed with water, and dried over sodium sulfate. The solvent was evaporated to give 1.10 g of crude product, which was purified by recrystallization from hexane to give pure product as yellow solid. Yield: 0.65 g (65%). ^{1}H NMR (250 MHz, $CDCl_3$): δ [ppm] 0.89 (12H, t, J = 7.3 Hz), 1.24−1.40 (16H, overlapped peaks), 1.62 (2H, m, M = 5, J = 7.3), 2.71 (4H, d, J = 6.7 Hz), 6.65 (2H, d, J = 3.7 Hz), 6.96 (2H, d, J = 3.1 Hz), 6.96 (2H, d, J = 3.1 Hz), 6.98 (2H, d, J = 3.1 Hz), 7.02 (2H, d, J = 3.7 Hz). ^{13}C NMR (125 MHz, $CDCl_3$): δ [ppm] 10.82, 14.13, 22.99, 25.49, 28.86, 32.35, 34.13, 41.39, 123.26, 123.50, 123.97, 125.89, 134.66, 135.31, 136.72, 144.20. Calcd. (%) for $C_{32}H_{42}S_4$: C, 69.26; H 7.63; S 23.11. Found: C 69.37; H 7.66; S 23.06.

1,3-*Bis*[11-(5‴-hexyl-2,2′:5′,2″:5″,2‴-quaterthiophen-5-yl)-undecyl]-1,1,3,3-tetramethyldisiloxane (**D2-Und-4T-Hex**) was synthesized from 5-hexyl-5‴-(undec-10-en-1-yl)-2,2′:5′,2″:5″,2‴-quaterthiophene and 1-[11-(5‴-hexyl-2,2′:5′,2″:5″,2‴-quaterthiophen-5-yl)undecyl]-1,1,3,3-tetramethyldisiloxane by hydrosilylation reaction:

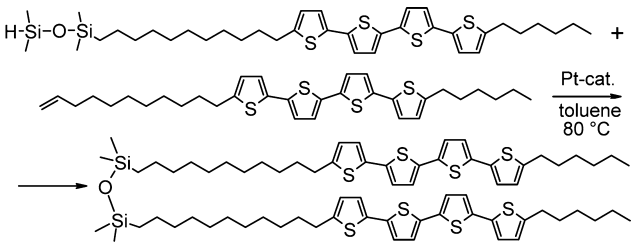

The detailed synthetic procedure is described below:

5-Hexyl-5‴-(undec-10-en-1-yl)-2,2′:5′,2″:5″,2‴-quaterthiophene (440 mg, 0.78 mmol) and 1-[11-(5‴-hexyl-2,2′:5′,2″:5″,2‴-quaterthiophen-5-yl)undecyl]-1,1,3,3-tetramethyldisiloxane (545 mg, 0.78 mmol) were dissolved in 50 mL of anhydrous toluene under argon, and 50 μL of Karstedt's catalyst was then added. The reaction was complete after the solution was stirred at 80 °C for 8 h. The reaction yield according to GPC analysis was 57%. The crude product was purified by preparative GPC in 30% isolated yield. ^{1}H NMR (250 MHz, $CDCl_3$): δ [ppm] 0.04 (12H, s), 0.52 (4H, t, J = 7.5 Hz), 0.92 (6H, t, J = 6.9 Hz), 1.25−1.45 (44 H, overlapping peaks with maximum at 1.27 ppm), 1.69 (8H, m, J = 7.5 Hz), 2.78 (8H, t, J = 7.5 Hz), 6.68 (4H, d, J = 3.7 Hz), 6.94−7.00 (8H, overlapping peaks), 7.03 (4H, d, J = 3.7 Hz). ^{13}C NMR (75 MHz, $CDCl_3$): δ [ppm] 0.42, 22.55, 23.33, 28.77, 29.14, 29.39, 29.42, 29.58, 29.61, 29.70, 30.24, 31.54, 31.58, 33.42, 123.47, 123.62, 124.06, 124.83, 134.57, 135.53, 135.54, 145.73. ^{29}Si NMR (60 MHz, $CDCl_3$): δ [ppm] 7.63.

Methods. Differential scanning calorimetry (DSC) was performed with a Mettler DSC-822e instrument at a scanning rate of 10 °C.min^{-1} in argon.

X-ray diffraction experiments (XRD) at room temperature were conducted on oriented fibers using a custom-built SAXS/WAXS machine coupled to a Rigaku MicroMax-007 HF rotating anode generator (λ =1.54 Å). The size of the point-like X-ray beam on the sample was approximately 300 μm. The 2D

dx.doi.org/10.1021/jp307054r | J. Phys. Chem. C 2012, 116, 22727−22736

WAXS data were collected using X-ray sensitive Fuji image plates with the pixel size of 100 × 100 μm^2. SAXS data were recorded with a 2D multiwire detector. Variable-temperature XRD measurements were carried out in a Linkam heating stage operating under nitrogen flow. The modulus of the scattering vector s ($s = 2\sin\theta/\lambda$, where θ is the Bragg angle) was calibrated using three diffraction orders of silver behenate. The hole in the center of the image plate allows performing simultaneous SAXS and WAXS measurements.

High-resolution variable-temperature powder X-ray diffraction patterns were recorded using SAXS- and WAXS S3-Micropix camera (CuK_α radiation, λ = 1.542 Å), manufactured by Hecus X-ray Systems Gmbh., Graz, Austria. Scattered beam was registered by one of the two detectors: either two-dimensional Pilatus 100K or linear gas position sensitive detector PSD 50M, the high-voltage and current at Xenocs Genix generator were 50 kV and 1 mA. The exposure time was varied from 600 to 5000 s. For temperature experiments, Peltier element (in the range from −5 to 120 °C) or Joule heater (from 23 to 300 °C) were used.

Variable-temperature X-ray diffraction on oriented samples was carried out on beamline BM26 at the European Synchrotron Radiation Facility in Grenoble, France, using 10 keV X-ray photons. The data were collected in transmission geometry using a FreLoN Kodak CCD detector positioned at 15 cm. The temperature was controlled by a Linkam heating stage. The modulus of the scattering vector s ($s = 2(\sin\theta)/\lambda$, where θ is the Bragg angle and λ is the wavelength) was calibrated using silver behenate. Fibers with a diameter of 0.7 mm were obtained by extruding the material at 70 °C with a home-build mini-extruder. The experiments were performed during heating and cooling cycles at 10 °C·min^{-1}.

Density measurements were performed by flotation method using aqueous potassium iodide solutions of different concentrations as reference solutions. The accuracy of density measurements is 0.01 g/cm^3.

Charge carrier mobilities have been measured in OFETs prepared form **D1-Und-4T-Hex**, **D1-Und-4T-EH**, and **D4-Und-4T-EH** by solution processing as described elsewhere.[13] OFET from **Hex-4T-Hex** and **EH-4T-EH** were prepared by vacuum sublimation. The data for vacuum-sublimed **Dec-4T-Dec** and solution-processed **D4-Und-4T-Hex** were taken from the literature.[3c,12]

RESULTS AND DISCUSSIONS

Structure and Phase Behavior of α, α′-Dialkylquaterthiophenes. To understand the impact of the lateral chain architecture on the crystal structure of α,α′-dialkylquaterthiophenes and their electronic properties, the phase behavior of linear and branched compounds was analyzed during heating.

At room temperature, oriented fibers of **Hex-4T-Hex** possess a well-organized crystal phase (Form I) with 3D order (cf. Figure 3a). The lattice parameters of Form I are found to be close to the ones previously reported.[17] At 86 °C, one can clearly observe a change in X-ray patterns corresponding to a phase transition (cf. Table 1 and Figure 4a): a number of reflections disappear, while some others change the intensity. The presence of narrow reflections in the wide-angle range indicates the formation of a new crystal phase (Form II) rather than a smectic phase, as it was assumed previously.[15] Only above 176 °C, the crystalline peaks completely disappear leaving a broad amorphous halo. The details of the crystal packing will be discussed below.

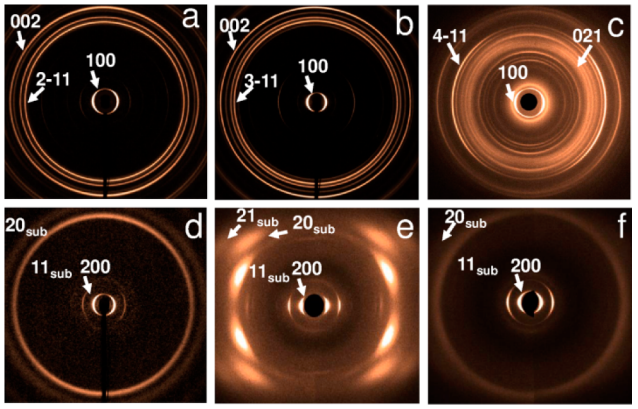

Figure 3. 2D X-ray diffraction patterns of **Hex-4T-Hex** (a), **Dec-4T-Dec** (b), **EH-4T-EH** (c), **D2-Und-4T-Hex** (d), **D2-Und-4T-EH** (e), and **D4-Und-4T-EH** (f) measured at room temperature. The fiber direction is vertical.

The increase of the aliphatic chain length to ten carbon atoms in **Dec-4T-Dec** leads to an increase of the temperature and enthalpy of the first transition (cf. Table 1), whereas the isotropization enthalpy does not change.[17] At room temperature, **Dec-4T-Dec** is in the crystalline state (cf. Figure 3b), the unit cell parameters being a = 37.93 Å, b = 5.99 Å, c = 7.79 Å, γ = 93.2° (cf. Table 1). Compared to **Hex-4T-Hex**, the increased a-parameter can be accounted for by longer aliphatic chains, while the other unit cell parameters are virtually the same. During heating of **Dec-4T-Dec** fibers, a transition from Form I to Form II crystal was observed at a higher temperature as compared to **Hex-4T-Hex** (98 °C vs 81 °C) (cf. Figure 4b). The transition temperatures revealed by XRD are in good agreement with those obtained by DSC (cf. Table 1). The increase of the temperature and enthalpy of the low-temperature transition in **Dec-4T-Dec** as compared to **Hex-4T-Hex** indicates stabilization of the Form I crystals due to longer alkyl chains, allowing for their better packing and subsequent ordering of **4T** segments in their usual sublattice. A decrease of the melting point with the increase of the side group length is typical for example for regioregular poly(3-alkyl thiophenes). (cf. ref 18 and references therein) In contrast, the isotropization point tumbles with the increase of alkyl end group length. It is noteworthy that the presence of conformational defects of the alkyl chains can be inferred from a decrease of a-parameter of Form II as compared to Form I (cf. Table 1).

It is important to emphasize that the crystal destabilization by the end alkyl tails can be induced not only by temperature but also by changing the alkyl chain architecture, e.g., by introducing a branching point. The DSC data of **EH-4T-EH** with branched α,α′-*bis*(2-ethylhexyl) groups reveals a drastic decrease of both the first and second phase transition temperatures to 34 and 108 °C, respectively (cf. Table 1). This is probably due to a substantial shift of balance between the rigid quaterthiophene core and bulkier branched alkyl groups. While these transitions are thermally reversible, the transformation from one phase to the other is characterized by a considerable temperature hysteresis.

The analysis of room-temperature X-ray diffractograms of **EH-4T-EH** (cf. Figure 3c) reveals a monoclinic crystalline lattice (symmetry group P21/b) with the following parameters: a = 19.68 Å, b = 11.45 Å, c = 7.35 Å, γ = 92.7° (Form I). The corresponding table with peaks indexation is given in the Supporting Information. In contrast to compounds with linear

dx.doi.org/10.1021/jp307054r | J. Phys. Chem. C 2012, 116, 22727−22736

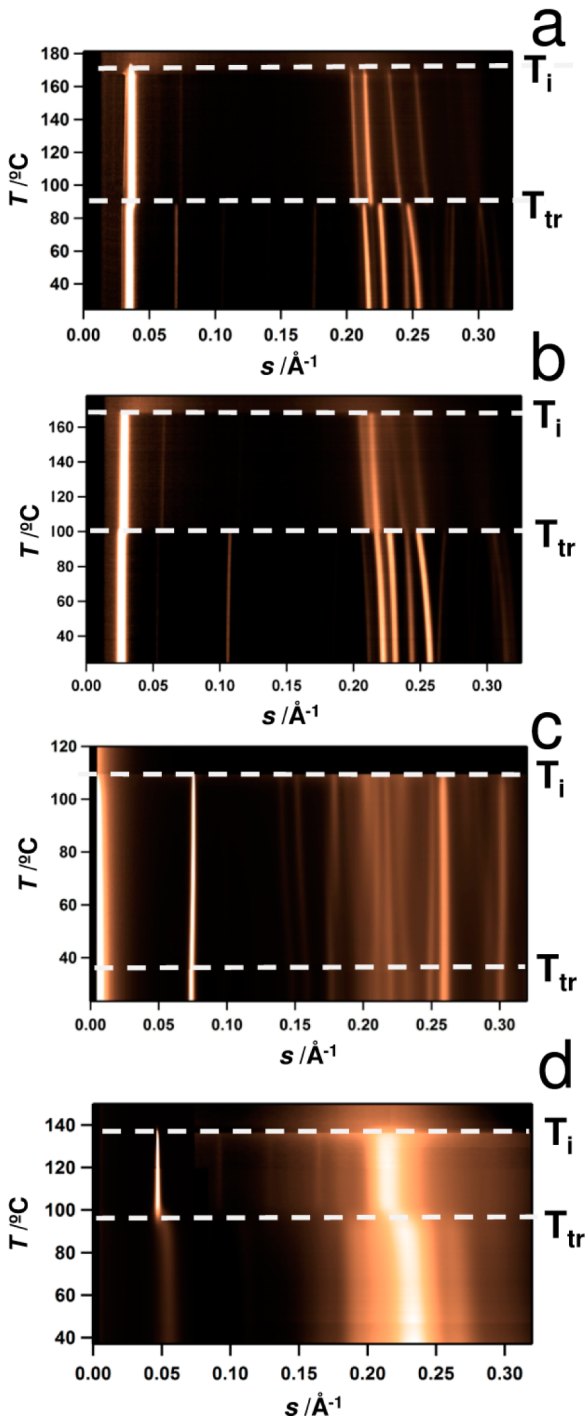

Figure 4. Change of X-ray patterns XRD on heating of **Hex-4T-Hex** (a), **Dec-4T-Dec** (b), **EH-4T-EH** (c), and **D2-Und-4T-EH** (d) fibers at a rate of 10 °C/min. The dashed lines indicate temperatures of phase transitions in the corresponding materials (cf. text for more details).

aliphatic chains, which do not have a tilt of the end groups with respect to quaterthiophene fragments, the molecular conformation of **EH-4T-EH** is not straight. This is probably due to a strong mismatch between the thiophene and 2-ethylhexyl cross sections (cf. the corresponding molecular model in Figure 5a). On the basis of the azimuthal positions of the two characteristic thiophene reflections at 4.63 Å and 3.94 Å, the tilt angle of quaterthiophene blocks with respect to 100-direction

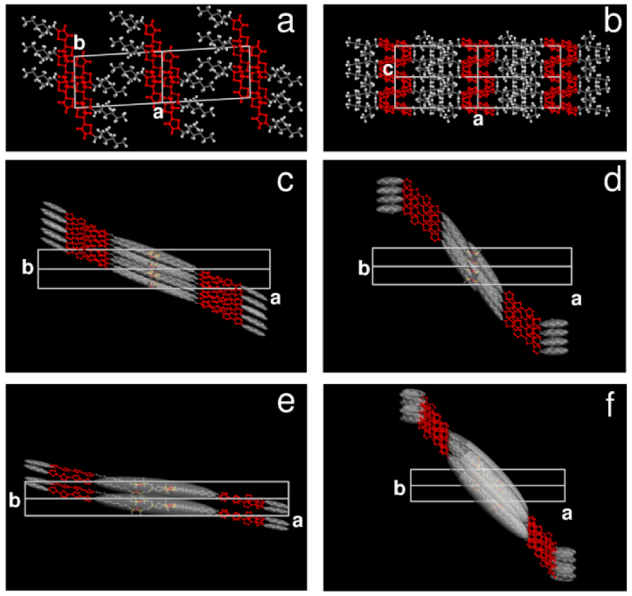

Figure 5. Schematic representations of the molecular arrangement in the unit cells of the studied compounds: ab- (a) and ac- (b) projections of **EH-4T-EH**, ab-projection for **D2-Und-4T-Hex** (c), **D2-Und-4T-EH** (d), **D4-Und-4T-Hex** (e), and **D4-Und-4T-EH** (f). The semitransparent gray envelopes denote the conformationally disordered parts of the molecule. For the last four models, the hydrogens are omitted for simplicity.

was estimated to be 58°. The tilt angle of the alkyl chains of 21° was calculated from minimized molecular model. It was found that for better packing, the branched alkyls have to form a layer with interdigitation (Figure 5a,b). The tilt angle of the alkyl chains in **EH-4T-EH** is close to the molecular tilt of linear hexyl groups in **Hex-4T-Hex**, i.e., 22° (cf. Figure 2a). Consequently, the arrangement of α,α'-dialkylsubstituted quaterthiophenes in the unit cell is largely determined by the alkyl groups packing.

Above the transition temperature of 34 °C, **EH-4T-EH** remains crystalline, with a slightly decreased a-parameter (cf. Figure 4c, Table 1). A detailed analysis of the wide-angle peak positions reveals a significant increase of the thermal expansion coefficient in the **bc**-plane above the transition. Minor changes in the WAXS pattern above the transition and the small enthalpy of the transition indicate that in this case the molecular rearrangements associated with the phase transition are much less significant than for the compounds with linear chains described above. The branching point in the aliphatic chains plays the role of a conformational defect in Form II of **Hex-4T-Hex** resulting in significant depression of melting temperature. However, the strong segregation of **4T** blocks preserves the global 3D ordering upon local reorganization of alkyl groups occurring at the first phase transition temperature.

Structure and Phase Behavior of Tetramethyldisiloxane-Based Dimers of α,α'-Dialkylquaterthiophenes. Introduction of flexible *bis*-(undecylene)tetramethyldisiloxane junction in the molecular structure significantly changes the ability of the quaterthiophene segments to self-organize. In this section, a comparative analysis of the structure and phase behavior of α,α'-dialkylquaterthiophene dimers with both linear (**D2-Und-4T-Hex**) and branched (**D2-Und-4T-EH**) terminal aliphatic groups will be presented.

The DSC curves of **D2-Und-4T-Hex** reveal two phase transitions at 75 and 190 °C, the latter being much more

dx.doi.org/10.1021/jp307054r | J. Phys. Chem. C 2012, 116, 22727−22736

pronounced than the former (Figure 6, curve 1). The temperature of the first transition is very close to that of

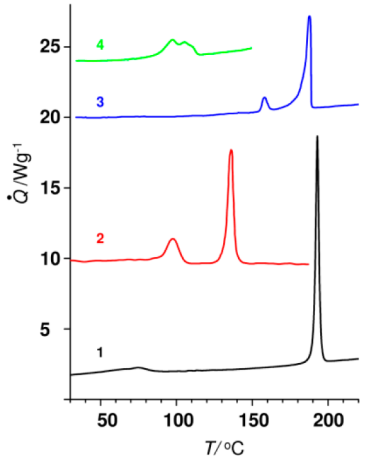

Figure 6. DSC heating scans of D2-Und-4T-Hex (1), D2-Und-4T-EH (2), D4-Und-4T-Hex (3), and D4-Und-4T-EH (4).

Hex-4T-Hex, though its enthalpy is five times smaller. Thus, the rearrangement of molecules in this case should be not so important, probably due to the presence of flexible tetramethyldisiloxane junction. At room temperature, the WAXS patterns reveal three characteristic reflections of the **4T** sublattice (cf. Figure 7, curve 1). In the small-angle region,

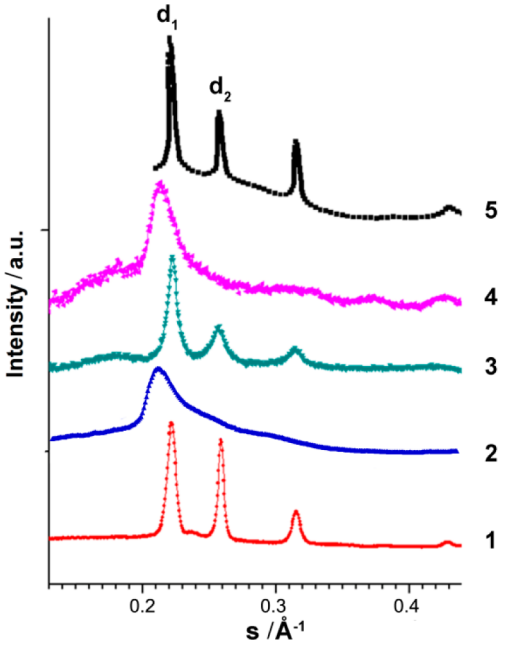

Figure 7. Room-temperature WAXS patterns, obtained for bulk **D2-Und-4T-Hex** (1), **D2-Und-4T-EH** (2), **D4-Und-4T-Hex** (3), and **D4-Und-4T-EH** (4). The WAXS curve of oligothiophene (5) is given for the sake of comparison.[14].

one can see a peak at 73.7 Å (cf. Table 1), the *d*-spacing of which is smaller than the fully extended molecular length. It is noteworthy that this peak appears in the diffractograms upon annealing the sample at elevated temperature, which shows that the complex molecular architecture of the dimer slows down the crystallization kinetics. However, even upon annealing, the absence of sharp reflections with mixed indices (cf. Figure 3d) except the ones of polythiophene indicates on significant disorder in the alkyl chain layer (Figure 3d). Therefore, the room temperature structure is assigned to an ordered smectic phase, and the regions with conformational disorder in the corresponding molecular model are schematically shown with semitransparent ellipsoids (cf. Figure 5c).

Above the first thermal transition (70 °C), the peak of the ordered smectic phase disappears, and one observes two orders of reflection corresponding to the distance of 40.5 Å (cf. Table 1). This spacing equals the distance between successive **4T**-blocks in the **D2-Und-4T-Hex** molecule, i.e. approximately one-half of the molecular length. Since the quaterthiophene sublatttice peaks are absent from the diffractogram recorded in this temperature range, the Form II phase was assigned to a disordered smectic phase (cf. Table 1).

Replacement of linear aliphatic end groups by branched ones significantly changes the structure and thermal behavior of the dimer. The DSC heating curve of **D2-Und-4T-EH** with branched aliphatic end chains displays two endothermic peaks at 98 and 136 °C (cf. curve 2 in Figure 6). One can see from Table 1 and Figure 6 that the temperature and enthalpy of the low-temperature phase transition for **D2-Und-4T-EH** is much higher than that for **EH-4T-EH** monomer. The isotropization point of **D2-Und-4T-EH** is higher as well. This change can be due to the presence of linear undecyl fragment on one end of the **4T** block, which allows it to form a more perfect crystalline lattice.

The 2D XRD pattern of **D2-Und-4T-EH** recorded at room temperature (Figure 3e) displays several orders of narrow equatorial reflections. In addition, broad and diffuse off-meridional reflections of the **4T** sublattice (cf. Table 2) are visible, which means that the structure incorporates small quaterthiophene crystallites. The pattern reveals a pseudomonoclinic unit cell (symmetry group P21) with the following parameters: a = 60.4 Å, b = 5.5 Å, c = 11.2 Å, γ = 90°. The calculated crystal density −1.11 g·cm^{-3} is in good agreement with the experimental one (1.12 g·cm^{-3}). The azimuthal positions of the **4T** sublattice reflections show that the quaterthiophenes are inclined by 43° with respect to 100-direction. The decrease of the tilt angle as compared to the **EH-4T-EH** compound is induced by the increase of the quaterthiophene cross-section resulting from looser local packing. On the basis of the significant width of the quaterthiophene sublattice peaks on the diffractogram of **D2-Und-4T-EH**, it is reasonable to assume that the limited spatial correlations in certain directions are due to disturbance of the quaterthiophenes packing by the bulky disiloxane groups. This assumption is proven by significant shift of sublattice reflexes to smaller angles compare to the molecules with linear end groups (Figure 7, curve 2). The resulting structure of the material at room temperature can be viewed as alternation of quaterthiophene crystalline layers with conformationally disordered layers of the alkyl chains (cf. Figure 5d). However, to achieve such relatively high crystal density, it is unlikely that the unit cell incorporates many conformational (e.g., folded molecules, kinks) or translational defects (e.g., relative shift of the molecules by half of the stacking period). The partially ordered packing of linear alkyl groups gives a characteristic peak at 4.6 Å with azimuthal position related to the tilt angle. The absence of azimuthal doubling of the reflection at 4.6 Å on diffractograms proves that the tilt angles of quaterthiophenes and undecylene blocks are close. On the basis of the proposed conformation of

dx.doi.org/10.1021/jp307054r | J. Phys. Chem. C 2012, 116, 22727−22736

Table 2. Packing Efficiency of the Quaterthiophene Blocks and Charge Carrier Mobility (μ)

sample	ρ_{exp} (gcm^{-3})	ρ_{calc} (gcm^{-3})	d_1 (Å)	d_2 (Å)	S (Å^2)	tilt angle[a] (deg)	μ (cm^2 V^{-1} s^{-1})
4T[23]		1.50	4.55	3.93	43.0	26	0.0001
polythiophene[17]		1.56	4.52	3.90	43.2		
EH-4T-EH	1.15	1.13	4.63	3.94	44.1	58	0.02[c]
Hex-4T-Hex[20]	1.19	1.22	4.59	3.91	43.2	22	0.02[c]
Dec-4T-Dec	1.15	1.15	4.50	3.89	42.0	22	0.1[c]
D2-Und-4T-EH	1.12	1.11	4.66	4.04	45.1	43	
D2-Und-4T-Hex	1.08	1.11[b]	4.53	3.99	43.0	25	0.003[d]
D4-Und-4T-EH	1.11		4.68	4.05	45.5	~50[e]	0.0004[d]
D4-Und-4T-Hex	1.12		4.56	3.86	42.7	<20	0.02[d]

[a]The tilt angle is calculated with respect to the 100 direction. [b]For smectic phase the density was estimated from a-parameter, **4T** sublattice parameters and the tilt angle. [c]Measured in devices prepared by vacuum sublimation. [d]Measured in devices prepared by solution processing. [e]The tilt angle estimated for the case of siloxane and undecyl fragments to be parallel to **4T** blocks.

the central part of the molecule, the inclination of branched 2-ethylhexyl end groups can be estimated from the contour length of each molecular fragment. The found value of 18° is close to that of the end groups of **EH-4T-EH**.

The high-temperature WAXS data show that the phase transition of **D2-Und-4T-EH** to Form II at 98 °C (cf. Figure 4d and Table 1) brings about sharpening of the smectic peaks and disappearance of the quaterthiophenes sublattice peaks. Therefore, similar to the case of **D2-Und-4T-Hex**, the high temperature phase can be assigned to a disordered smectic.

Structure and Phase Behavior of Carbosilane-Siloxane-Based Tetramers of α,α'-Dialkylquaterthiophenes. The isotropization temperature of hexyl-terminated tetramer **D4-Und-4T-Hex** (187 °C) is very close to that of the corresponding dimer, i.e., **D2-Und-4T-Hex**, (cf. Figure 6), but the first thermal transition for the tetramer occurs at a much higher temperature (160 °C). Such improvement of the Form I stability is probably related to flexibility of carbosilane-siloxane junction that allows to better adjusting the thiophene and alkyl layers at high temperature. The SAXS curves of **D4-Und-4T-Hex** at room temperature exhibit coexistence of ordered smectic phase with characteristic interlayer distance of 79.4 Å (cf. peak I in Figure 8) and disordered smectic phase with a spacing of 46.1 Å (cf. peak II in Figure 8). In this case, it is clear that peak II is not the second order of peak I, as it has a bigger

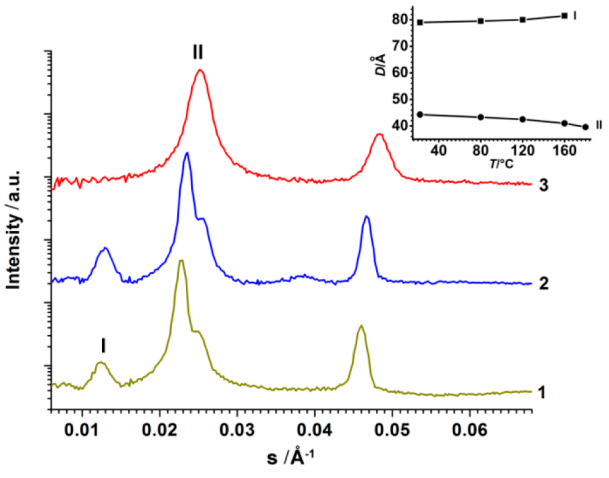

Figure 8. SAXS curves of the as-received **D4-Und-4T-Hex** (1), on heating at 120 °C (2), 170 °C (3). The inset shows the temperature dependence of *d*-spacings corresponding to the ordered (**I**) and disordered (**II**) smectic phase reflections.

d-spacing. The WAXS patterns of the compound are dominated by the **4T** sublattice reflections (cf. curve 3 in Figure 7).

Heating of the **D4-Und-4T-Hex** sample leads to a substantial shift of the wide-angle reflection to smaller angles, which can be accounted for by the thermal expansion of the **4T** sublattice (not shown here). The same trend is exhibited by peak I (cf. inset in Figure 8). By contrast, the reflections of the disordered smectic phase steadily shift during the overall heating process in the opposite direction, with eventual interlayer distance of 42.7 Å at 180 °C (cf. inset in Figure 8). Such contraction on heating is typical for the lattice parameters of thermotropic liquid crystalline systems.[19] At 160 °C, the crystalline reflections of the sublattice completely disappear from the diffractograms marking the melting point of the ordered smectic phase. On the basis of the described features of the X-ray patterns, it is assumed that in the unit cell of **D4-Und-4T-Hex** the molecules adopt an X-shape conformation (Figure 5e). The molecular inclination with respect to 100-direction cannot be found directly. However, a small difference between a-parameter and the contour length of **D4-Und-4T-Hex** allows concluding that for the fully extended conformation this angle is below 20°.

The thermal behavior of **D4-Und-4T-EH** is similar to that of **D4-Und-4T-Hex** (Figure 6, Table 1). However, the izotropization temperature for the compounds with branched alkyl tails was found to be somewhat lower than that for the dimer and tetramer with linear end groups (i.e., 136 °C for **D2-Und-4T-EH** and 115 °C for **D4-Und-4T-EH**). The higher melting temperature of dimers compared to tetramers, can be explained by a defect-inducing role of branching point in tetramers. As compared to **D4-Und-4T-Hex**, the temperature window for the disordered smectic phase of **D4-Und-4T-EH** is narrower because of the destabilizing effect of the bulky end groups.

The room-temperature SAXS patterns of **D4-Und-4T-EH** reveal much similarity with the ones of **D4-Und-4T-Hex** (cf. Figure 9). Indeed, the patterns consistently show that the two phases, i.e., the ordered and disordered smectic phases, coexist at room temperature, which means that the formation of the ordered smectic phase on cooling was not complete. The room-temperature WAXS pattern of a **D4-Und-4T-EH** fiber reveal two broad wide-angle reflections with the characteristic *d*-spacings of the **4T** sublattice. Similar to **D2-Und-4T-EH**, the WAXS reflexes are shifted to small-angle direction because of disturbance of **4T** sublattice (Figure 7, curve 4). The misorientation of the quaterthiophene reflections can be explained by the presence of the flexible tetramethyldisiloxane central part, which weakens the orientational correlations between the neighboring **4T** segments. Therefore, the precise

dx.doi.org/10.1021/jp307054r | J. Phys. Chem. C 2012, 116, 22727−22736

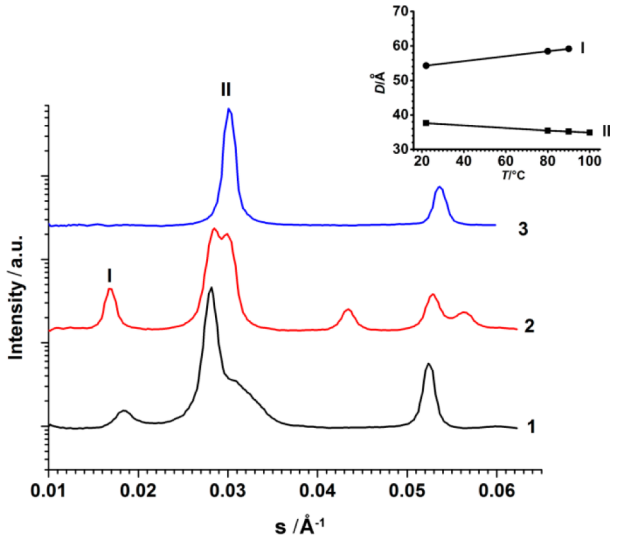

Figure 9. SAXS curves of as-received **D4-Und-4T-EH** measured at room temperature (1), and during heating at 80 °C (2) and 100 °C (3). The inset shows the temperature dependence of *d*-spacings corresponding to the ordered (**I**) and disordered (**II**) smectic phase reflections.

determination of the tilt angles of the different molecular segments is rather difficult, and can mainly be done from the smectic layer spacings (cf. Figure 5f).

The structural characteristics of the studied samples show that stability of the ordered state is mainly determined by aggregation of the quaterthiophene units. Despite the complex branched architecture of the compounds investigated, after annealing at high temperature the sublattice of quaterthiophenes can be identified in all the samples, with molecular packing close to that found for nonsubstituted quaterthiophenes. This is an interesting finding in view of applications of these molecules in the form of thin films and even monolayers for OFETs. The structure of thin films will be discussed in detail in a forthcoming publication. As mentioned above, the alkyl periphery can play both stabilizing and destabilizing roles for the quaterthiophenes packing. In the following section, the details of molecular packing will be discussed by considering the sublattice cross-section in the plane normal to the molecular axes.

Efficiency of the Quaterthiophenes Local Packing and Charge Carrier Mobility. In the studied compounds, the quaterthiophene segments form a typical "herring-bone" arrangement. For such centered lattice containing two molecules the 11 (d_1) and 20 (d_2) reflections are the most intense. Supposing that the sublattice projection on the plane normal to the molecular axis is close to rectangular (which is always the case) the cross-sectional area S can be computed as follows:

$$S = \frac{4d_2^2 d_1}{\sqrt{4d_2^2 - d_1^2}} \quad (1)$$

In Table 2, the values of *S* are summarized together with the experimental and calculated crystal density. The nonsubstituted quaterthiophene (4T) and nonsubstituted polythiophene were chosen as references. Generally, one can expect that the ideal packing of quaterthiophene blocks of the substituted compounds will result in S-values, which are close to those of **4T** and polythiophene, because of the end group effect. For all of the samples a good agreement between the experimental and calculated density is observed. The small differences can be attributed to the presence of a disordered smectic phase at room temperature, as was discussed above for the case of tetramers.

From the analysis of S-values several conclusions can be drawn. First, the chain packing is better for compounds with linear end groups as compared to their branched analogues. This can be explained by difficulties in accommodation of the bulky peripheral chains. Second, in the series of molecules with linear end groups the area per chain decreases from **Hex-4T-Hex** to **D4-Und-4T-Hex**. This fact is probably related to the increase of the driving force for segregation between the thiophene and alkyl blocks. Another reason is the presence of a disordered smectic phase for the dimer and tetramer during cooling from the isotropic state prior to crystallization which provides conditions for improved packing. A similar effect is known in the field of semicrystalline polymers when the crystallization process occurs from the mesophase. It is for example well documented that under these crystallization conditions, the crystallinity of such main-chain LC polymers as polyethylene or poly(dialkyl siloxanes) can approach 100%.[20−22]

In contrast to the molecules with linear end groups, the area per chain increases from **EH-4T-EH** to **D4-Und-4T-EH**. This trend can be explained by kinetic reasons. We speculate that crystallization of the compounds passes through several stages characterized by different degrees of regularity: disordered melt, disordered smectic phase, ordered smectic phase, and eventually the thermodynamically stable crystal. Thus, the final structure of the material strongly depends on its thermal history. It is clear that the presence of junctions and branching points, which can be considered as topological defects, hinders the local organization process. The standard sample preparation procedure employing extrusion of fibers, used in this work, does not always allow reaching the equilibrium crystal phase. Finally, a certain mixture of stable and metastable polymorphs can be present in the sample. In the smectic state, the material can form large monodomains (up to hundreds of micrometers large), which is important for fabrication of OFETs with reproducible properties. Consequently, the optimal chemical structure should provide the right balance between good packing of the thiophene blocks and the ability of the material to undergo "soft" self-assembly.

In Table 2, the characteristic values of charge carrier mobilities measured in OFETs are given. It is noteworthy that the highest mobility of 0.1 $cm^2V^{-1}s^{-1}$ was reported for quaterthiophene with long decyl groups **Dec-4T-Dec** having the lowest S-value of 42.0 $Å^2$, while one of the lowest values of mobility μ = 0.0004 $cm^2V^{-1}s^{-1}$ was observed for the tetramer with branched 2-ethylhexyl groups having the largest S-value of 45.5 $Å^2$. The absence of measurable field-effect mobility for **D2-Und-4T-EH** can be attributed not only to the high value of S = 45.1 $Å^2$, but also to high inclination of the **4T**-units in this structure (43°). The high tilt angle of the semiconducting **4T**-units is not favorable for OFETs, since it prohibits the efficient charge injection from the contacts and should increase the hopping barrier between the domains having different orientation in the polycrystalline film.

It is instructive to compare pairs of compounds having similar chemical structures. For instance, for quaterthiophenes with linear hexyl and decyl groups **Hex-4T-Hex** and **Dec-4T-**

dx.doi.org/10.1021/jp307054r | J. Phys. Chem. C 2012, 116, 22727−22736

Dec the value of S decreases from 43.2 to 42.0 Å^2, which corresponds to increase in mobility value from 0.02 to 0.1 cm^{2}V^{-1}s^{-1}. Similarly, the decrease of the S-value from 45.5 to 42.7 Å^2 for tetramers with branched 2-ethylhexyl and linear hexyl groups **D4-Und-4T-EH** and **D4-Und-4T-Hex**, respectively, corresponds to the increase of the OFET mobility from 0.0004 to 0.02 cm^{2}V^{-1}s^{-1}. Thus, a clear correlation between the calculated cross-sectional area and charge carrier mobilities is observed.

CONCLUSIONS

In the present work, a comparative analysis of the structure and thermal behavior of α,α'-dialkylsubstituted quaterthiophenes with different alkyl end groups and their organosilicon multipods has been carried out. The chemical structure of the alkyl periphery is found to play an important role in the molecular packing and thermal stability of the ordered phase. For quaterthiophenes with linear end groups, the temperature of transition from the ordered to disordered smectic phase decreases with the increase of the end group length, which testifies to the crucial role of the alkyl periphery. Moreover, the packing of alkyl chains can be hindered by introducing branching points of different nature. In particular, the quaterthiophenes with 2-ethylhexyl end groups adopt a zigzag conformation in the crystalline state at room temperature. This change of conformation leads to a significant decrease of the polymorphic transition and isotropization temperatures.

For all of the studied quaterthiophene-containing organosilicon dimers and tetramers the formation of quaterthiophene crystal sublattice was observed. This is likely to be promoted by a good phase separation between the blocks. However, the packing quality and tilt angle with respect to *a*-axis are determined by the structure of the surrounding alkyl network. For the tetramers, the limited molecular mobility is likely to hinder the material ordering. Therefore, the tetramer samples at room temperature exhibit coexistence of the ordered and disordered smectic phases.

On the basis of the structural data, the molecular models were proposed. The efficiency of quaterthiophenes packing in the sublattice was estimated from the molecular cross-section in the plane normal to the quaterthiophenes axis. The smallest cross-sectional area is pertinent to the quaterthiophene with decyl end groups **Dec-4T-Dec** and to the tetramer with linear hexyl groups **D4-Und-4T-Hex**. These molecules are also found to be most perspective for fabrication of the active layers in OFETs from the point of view of the charge carrier mobility. The tilt of the thiophene block with respect to the *a*-axis was also found to have a strong effect on the field-effect charge carrier mobility in thin films: an increase of the tilt angle results in a decrease of the mobility in solution-processed OFETs. It can be assumed that the large tilt angle of the semiconducting oligothiophene units prohibits efficient charge injection from the contacts and can increase the hopping barrier between the domains having different orientation in the polycrystalline film.

ASSOCIATED CONTENT

Supporting Information

Table with indexation of experimental reflections with corresponding calculated d-spacings for the Form I crystal of **EH-4T-EH**. This material is available free of charge via the Internet at http://pubs.acs.org.

AUTHOR INFORMATION

Corresponding Author

*E-mail: ponomarenko@ispm.ru (S.A.P.); dimitri.ivanov@uha.fr (D.A.I.).

Notes

The authors declare no competing financial interest.

ACKNOWLEDGMENTS

The authors acknowledge the French Agence Nationale de la Recherche for financial support in the frame of SPIRWIND project (HABISOL program) and T2T project (Blanc International program) and the Russian Ministry of Science and Education (Project for Financial Support of Leading Scientists No. 11.G34.31.0055 from 19.10.2011 and Project No. 11.519.11.6020).

REFERENCES

(1) Perepichka, I. F.; Perepichka, D. F. *Handbook of Thiophene-Based Materials: Applications in Organic Electronics and Photonics*; Wiley-VCH: Weinheim, Germany, 2009.

(2) Klauk, H. *Organic Electronics: Materials, Manufacturing and Applications*; Wiley-VCH: Weinheim, Germany, 2006.

(3) (a) Katz, H. E.; Lovinger, A. J.; Laquindanum, J. G. *Chem. Mater.* **1998**, *10*, 457. (b) Garnier, F.; Hajlaoui, R.; Kassmi, A.; Horowitz, G.; Laigre, L.; Porzio, W.; Armanini, M.; Provasoli, F. *Chem. Mater.* **1998**, *10*, 3334. (c) Halik, M.; Klauk, H.; Zschieschang, U.; Schmid, G.; Ponomarenko, S.; Kirchmeyer, S.; Weber, W. *Adv. Mater.* **2003**, *15*, 917.

(4) (a) Halik, M.; Klauk, H.; Zschieschang, U.; Schmid, G.; Radlik, W.; Ponomarenko, S.; Kirchmeyer, S.; Weber, W. *J. Appl. Phys.* **2003**, *93*, 2977. (b) Nagamatsu, S.; Kaneto, K.; Azumi, R.; Matsumoto, M.; Yoshida, Y.; Yase, K. *J. Phys. Chem. B* **2005**, *109*, 9374.

(5) Garnier, F.; Yassar, A.; Hajlaoui, R.; Horowitz, G.; Deloffre, F.; Servet, B.; Ries, S.; Alnot, P. *J. Am. Chem. Soc.* **1993**, *115*, 8716.

(6) (a) Locklin, J.; Li, D.; Mannsfeld, S. C. B.; Borkent, E.-J.; Meng, H.; Advincula, R.; Bao, Z. *Chem. Mater.* **2005**, *17*, 3366. (b) Ellinger, S.; Ziener, U.; Thewalt, U.; Landfester, K.; Müller, M. *Chem. Mater.* **2007**, *19*, 1070. (c) Kreyes, A.; Ellinger, S.; Landfester, K.; Defaux, M.; Ivanov, D. A.; Elschner, A.; Meyer-Friedrichsen, T.; Ziener, U. *Chem. Mater.* **2010**, *22*, 2079. (d) Defaux, M.; Gholamrezaie, F.; Wang, J.; Kreyes, A.; Ziener, U.; Anokhin, D. V.; Ivanov, D. A.; Moser, A.; Neuhold, A.; Salzmann, I.; et al. *Adv. Mater.* **2012**, *24*, 973. (e) Fritz, S. E.; Mohapatra, S.; Holmes, B. T.; Anderson, A. M.; Prendergast, C. F.; Frisbie, C. D.; Ward, M. D.; Toney, M. F. *Chem. Mater.* **2007**, *19*, 1355. (f) Mohapatra, S.; Holmes, B. T.; Newman, C. A.; Prendergast, C. F.; Frisbie, C. D.; Ward, M. D. *Adv. Funct. Mater.* **2004**, *14*, 605.

(7) Mishra, A.; Ma, C.-Q.; Bäuerle, P. *Chem. Rev.* **2009**, *109*, 1141.

(8) Allard, S.; Forster, M.; Souharce, B.; Thiem, H.; Scherf, U. *Angew. Chem., Int. Ed.* **2008**, *47*, 4070.

(9) Ma, C. Q.; Fonrodona, M.; Schikora, M. C.; Wienk, M. M.; Janssen, R. A. J.; Bäuerle, P. *Adv. Funct. Mater.* **2008**, *18*, 3323.

(10) Perepichka, I. F.; Perepichka, D. F.; Meng, H.; Wudl, F. *Adv. Mater.* **2005**, *17*, 2221.

(11) Ponomarenko, S. A.; Kirchmeyer, S. *Adv. Polym. Sci.* **2011**, *235*, 33.

(12) Ponomarenko, S. A.; Tatarinova, E. A.; Muzafarov, A. M.; Kirchmeyer, S.; Brassat, L.; Mourran, A.; Moeller, M.; Setayesh, S.; Leeuw, D. *Chem. Mater.* **2006**, *18*, 4101−4108.

(13) Troshin, P. A.; Ponomarenko, S. A.; Luponosov, Y. N.; Khakina, E. A.; Egginger, M.; Meyer-Friedrichsen, T.; Elschner, A.; Peregudova, S. M.; Buzin, M. I.; Razumov, V. F.; et al. *Sol. Energy Mater. Sol. Cells* **2010**, *94*, 2064.

(14) Samuelsen, E. J.; Mardalen, J. Structure of Polythiophenes, In: *Handbook of Conductive Molecules and Polymers: Conductive Polymers: Spectroscopy and Physical Properties*; Nalwa, H. S., Ed. ; John Wiley and Sons: London, U.K.,1997; Vol. 3 , Chapter 2.

(15) Amundson, K. R.; Katz, H. E.; Lovinger, A. J. *Thin Solid Films* **2003**, *426*, 140.
(16) Moret, M.; Campione, M.; Borghesi, A.; Miozzo, L.; Sassella, A.; Trabattoni, S.; Lotz, B.; Thierry, A. *J. Mater. Chem.* **2005**, *15*, 2444.
(17) Ponomarenko, S.; Kirchmeyer, S. *J. Mater. Chem.* **2003**, *13*, 197−202.
(18) *Handbook of Thiophene-Based Materials. Applications in Organic Electronics and Photonics: Synthesis and Theory*; Perepichka, I. F., Perepichka, D. F., Eds.; John Wiley and Sons Ltd.: New York, 2009; Vol. *1*, pp 194−195.
(19) Zhu, X.; Beginn, U.; Moeller, M.; Gearba, R. I.; Anokhin, D. V.; Ivanov, D. A. *J. Am. Chem. Soc.* **2006**, *128*, 16928.
(20) Ungar, G. *Polymer* **1993**, *34*, 2050.
(21) Defaux, M.; Vidal, L.; Moeller, M.; Gearba, R.; Dimasi, E.; Ivanov, D. A. *Macromolecules* **2009**, *42*, 3500.
(22) Gearba, R. I.; Anokhin, D. V.; Bondar, A. I.; Godovsky, Yu. K.; Papkov, V. S.; Makarova, N. N.; Magonov, S. N.; Bras, W.; Koch, M. H. J.; Masin, F.; et al. *Macromolecules* **2006**, *39*, 988.
(23) Siegrist, T.; Kloc, C.; Laudise, R. A.; Katz, H. E.; Haddon, R. C. *Adv. Mater.* **1998**, *10*, 379.